Inorg. Chem. **2004**, *43*, 613–621

Density Functional Study of a μ-1,1-Carboxylate Bridged Fe(III)–O–Fe(IV) Model Complex. 2. Comparison with Ribonucleotide Reductase Intermediate X

Wen-Ge Han,* Timothy Lovell,* Tiqing Liu, and Louis Noodleman*

Department of Molecular Biology, TPC15, The Scripps Research Institute, 10550 N. Torrey Pines Road, La Jolla, California 92037

Received October 28, 2002

Using broken-symmetry density functional theory, we have studied an experimentally proposed model for ribonucleotide reductase (RNR) intermediate X, which contains a single oxo bridge, one terminal H_2O or OH^- ligand, a bidentate carboxylate from Glu115, and a mono-oxygen bridge provided by Glu238. For the models proposed here, the terminal H_2O/OH^- ligand binds to site Fe1 which is closer to Tyr122. The diiron centers are assigned as high-spin Fe(III)Fe(IV) and antiferromagnetically coupled to give the $S_{total} = {}^1/_2$ ground state. Calculations show that the model with a terminal hydroxide in the antiferromagnetic $\{S_{Fe1} = 2, S_{Fe2} = {}^5/_2\}$ state (Fe1 = Fe(IV), Fe2 = Fe(III)) is the lowest energy state, and the calculated isomer shift and quadrupole splitting values for this cluster are also the best among the four clusters studied here when compared with the experimental values. However, the DFT-calculated ^{1}H proton and ^{17}O hyperfine tensors for this state do not show good agreement with the experiments. The calculated Fe1–Fe2 distances for this and the other three clusters at >2.9 Å are much longer than the 2.5 Å which was predicted by the EXAFS measurements. The mono-oxygen bridge provided by Glu238 tends to be closer to one of the Fe sites in all clusters studied here, and it does not function as a bridge in helping to produce a short Fe–Fe distance. Overall, the models tested here are not likely to represent the core structure of RNR intermediate X. The model with the terminal OH^- binding to the Fe1(III) center shows the best calculated ^{1}H proton and ^{17}O hyperfine tensors compared with the experimental values. This supports the earlier proposal based on analysis of ENDOR spectra (Willems et al.[16]) that the terminal oxygen group binds to the Fe(III) site in RNR-X.

1. Introduction

Ribonucleotide reductase (RNR) catalyzes the reduction of ribonucleotides to deoxyribonucleotides which are used in DNA biosynthesis.[1,2] "Class I" RNR contains a binuclear iron cluster in subunit R2 that undergoes oxygen activation to produce a free radical at tyrosine 122 (Tyr122). This radical functions as a "pilot light" which begins the catalytic reaction by a long-range proton coupled electron-transfer process to generate a thiyl radical on cystein 439 in another subunit R1, which then performs the nucleotide reduction.[3,4] Once the tyrosine radical is lost, the enzyme becomes inactive, but the active form can be regenerated through the following reaction cycle (see Figure 1):[5]

$$\mathrm{Fe(III)}(\mu\text{-O})(\mathrm{OH}_n)\mathrm{Fe(III)}-\mathrm{Tyr122}-\mathrm{OH} + 2\mathrm{e}^- + (4-n)\mathrm{H}^+ \rightarrow \mathrm{Fe(II)Fe(II)}-\mathrm{Tyr122}-\mathrm{OH} + 2\mathrm{H_2O} \quad \text{(I)}$$

$$\mathrm{Fe(II)Fe(II)}-\mathrm{Tyr122}-\mathrm{OH} + \mathrm{O_2} + \mathrm{e}^- + n\mathrm{H}^+ \rightarrow \mathrm{Fe(III)}(\mu\text{-O})(\mathrm{OH}_n)\mathrm{Fe(IV)}-\mathrm{Tyr122}-\mathrm{OH} \quad \text{(II)}$$

$$\mathrm{Fe(III)}(\mu\text{-O})(\mathrm{OH}_n)\mathrm{Fe(IV)}-\mathrm{Tyr122}-\mathrm{OH} \rightarrow \mathrm{Fe(III)}(\mu\text{-O})(\mathrm{OH}_n)\mathrm{Fe(III)}-\mathrm{Tyr122}-\mathrm{O}^\bullet + \mathrm{H}^+ \quad \text{(III)}$$

where $n = 1$ or 2 in eqs (I)−(III).

So far the structure for the active form of the protein with tyrosine radical is still unknown, but X-ray structures of RNR from *E. coli* are available in both reduced and oxidized(met)

* Corresponding authors. E-mail: wengehan@scripps.edu (W.-G.H.); tlovell@scripps.edu (T.L.); lou@scripps.edu (L.N.). Fax: (858) 784-8896.

(1) Wallar, B. J.; Lipscomb, J. D. *Chem. Rev.* **1996**, *96*, 2625−2657.
(2) Sjöberg, B. M. *Struct. Bonding* **1997**, *88*, 139−173.
(3) Sturgeon, B. E.; Burdi, D.; Chen, S.; Huynh, B. H.; Edmondson, D. E.; Stubbe, J.; Hoffman, B. M. *J. Am. Chem. Soc.* **1996**, *118*, 7551−7557.
(4) Stubbe, J.; van der Donk, W. A. *Chem. Biol.* **1995**, *2*, 793−801.
(5) Lovell, T.; Li, J.; Noodleman, L. *J. Biol. Inorg. Chem.* **2002**, *7*, 799−809.

10.1021/ic0206443 CCC: $27.50
Published on Web 12/24/2003

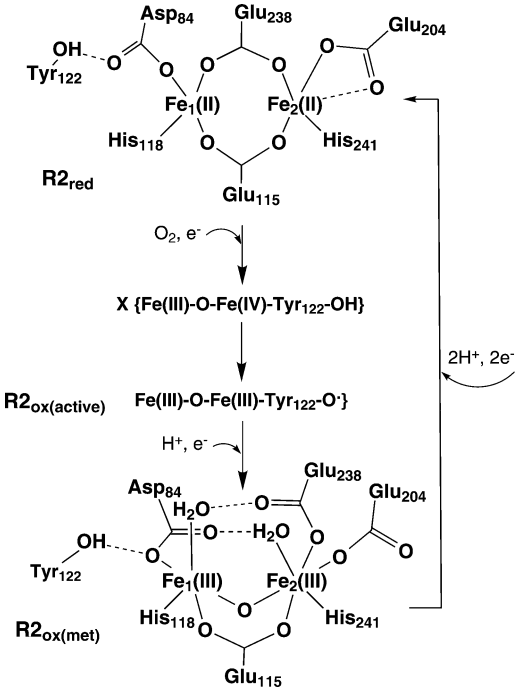

Figure 1. Schematic of the reaction cycle of formation of the active diferric cluster ($R2_{ox(active)}$) (with tyrosyl radical) from the reaction of O_2 with the diferrous cluster ($R2_{red}$). X is the intermediate state with Fe(III)−O−Fe(IV) centers. Water ligands and protons may enter or leave the active site.

forms (see Figure 1).[6−9] Here we assume that the first ligand shell structure of the active form of R2 is the same as that of the diferric(met) form, but with some cluster rearrangement possible (and addition or loss of waters and protons). Then in both the reduced and oxidized states, Fe1 (which is close to Tyr122) is ligated to the side chains of Asp84 and His118, and the other Fe (Fe2) is ligated to Glu204 and His241. In the diferrous cluster, both carboxylate groups from Glu238 and Glu115 exist in a bridging position between the two irons. Upon interaction with an O_2 molecule and the subsequent oxidation reaction, the carboxylate of Glu238 changes from the bidentate position to monodentate binding with Fe2. Meanwhile, a water molecule binds to Fe1, and this H-bonds with Glu238. One oxygen atom from O_2 is reduced to H_2O, and the other is incorporated as a bridging oxo in the diferric form. In addition, the carboxylate of Glu204 undergoes a shift from bidentate to monodentate ligation of Fe2. The carboxylate of Asp84 shifts from monodentate to approximate bidentate ligation of Fe1 with the production of Tyr122$^{\bullet}$ radical, and Asp84 also H-bonds with a water molecule coordinated to Fe2.

During the formation of active R2, a transient species (intermediate X) is formed (reaction II) which oxidizes tyrosine to the stable radical form (reaction III), as shown by ENDOR and Mössbauer hyperfine spectra.[10−13] Though there has been a significant experimental attempt to elucidate the structure of this short-lived catalytic species, the detailed structure of intermediate X is still not clear.[3,10,11,14−18] A combination of Q-band ENDOR and Mössbauer data indicates the iron centers of X are high spin Fe(III) ($S = {}^5/_2$) and high spin Fe(IV) ($S = 2$) sites that antiferromagnetically couple to give an $S_{total} = {}^1/_2$ ground state.[3] The best fit Mössbauer isomer shifts and quadrupole splittings on Fe were redetermined on the basis of accurate ^{57}Fe ENDOR hyperfine parameters as constraints. X is therefore presently described as a spin-coupled Fe(III)Fe(IV) center without a radical, but with significant spin delocalization onto the oxygen ligand-(s).[3] All experimental data support the existence of at least one μ-oxo bridge in the core structure of X.[14−19] A short Fe−Fe distance of 2.5 Å for X is implicated by the EXAFS measurements and data analysis in both wild-type and mutant Y122F proteins.[17] On the basis of this very short Fe−Fe distance, several possible core structures for X were proposed, each of which includes at least one μ-oxo bridge, and two monodentate or/and bidentate carboxylate bridges from Glu115 and Glu238.[17,19] Very recently, on the basis of their CW and pulsed Q-band ^{17}O-ENDOR experiments and the former ENDOR[16] and EXAFS[17] observations, Burdi et al.[18] proposed a structure for X, which contains two oxygen atoms, both initially derived from O_2, with one present as a μ-oxo bridge and one as a terminal aqua ligand bound to the Fe(III) site; one or two additional mono-oxygen bridges provided by the carboxylate oxygens of Glu115 and Glu238 may also be present.

One theoretical model of intermediate X has been proposed and examined by Siegbahn,[20] which contains (see Figure 6 in ref 20) one μ-oxo bridge, one hydroxo bridge, and two bidentate carboxylates from Glu115 and Glu238. Following geometry optimization of this $S_{total} = {}^1/_2$ model using the B3LYP density functional theory (DFT) approach,[20] an Fe−Fe distance of 2.61 Å was obtained. Furthermore, spin populations of 0.99 and −1.71 were noted for the two iron sites. Such small spin populations are more characteristic of low spin and intermediate spin Fe centers, rather than high spin Fe sites, and appear inconsistent with the ENDOR and Mössbauer data for X. In our first study of proposed RNR-X type species, we have examined this and related models using broken-symmetry density functional theory and spin-projec-

(6) Nordlund, P.; Sjöberg, B. M.; Eklund, H. *Nature* **1990**, *345*, 593−598.
(7) Nordlund, P.; Eklund, H. *J. Mol. Biol.* **1993**, *232*, 123−164.
(8) Nordlund, P.; Eklund, H. *Curr. Opin. Struct. Biol.* **1995**, *5*, 758−766.
(9) Logan, D. T.; Su, X. D.; Åberg, A.; Regnström, K.; Hajdu, J.; Eklund, H.; Nordlund, P. *Structure* **1996**, *4*, 1053−1064.
(10) Bollinger, J. M., Jr.; Edmondson, D. E.; Huynh, B. H.; Filley, J.; Norton, J. R.; Stubbe, J. *Science* **1991**, *253*, 292−298.
(11) Bollinger, J. M., Jr.; Stubbe, J.; Huynh, B. H.; Edmondson, D. E. *J. Am. Chem. Soc.* **1991**, *113*, 6289−6291.
(12) Ravi, N.; Bollinger, J. M., Jr.; Huynh, B. H.; Edmondson, D. E.; Stubbe, J. *J. Am. Chem. Soc.* **1994**, *116*, 8007−8014.
(13) Bollinger, J. M., Jr.; Tong, W. H.; Ravi, N.; Huynh, B. H.; Edmondson, D. E.; Stubbe, J. *J. Am. Chem. Soc.* **1994**, *116*, 8015−8023; 8024−8032.
(14) Burdi, D.; Sturgeon, B. E.; Tong, W. H.; Stubbe, J.; Hoffman, B. M. *J. Am. Chem. Soc.* **1996**, *118*, 281−282.
(15) Veselov, A.; Scholes, C. P. *Inorg. Chem.* **1996**, *35*, 3702−3705.
(16) Willems, J. P.; Lee, H. I.; Burdi, D.; Doan, P. E.; Stubbe, J.; Hoffman, B. M. *J. Am. Chem. Soc.* **1997**, *119*, 9816−9824.
(17) Riggs-Gelasco, P. J.; Shu, L.; Chen, S.; Burdi, D.; Huynh, B. H.; Que, L., Jr.; Stubbe, J. *J. Am. Chem. Soc.* **1998**, *120*, 849−860.
(18) Burdi, D.; Willems, J. P.; Riggs-Gelasco, P. J.; Antholine, W. E.; Stubbe, J.; Hoffman, B. M. *J. Am. Chem. Soc.* **1998**, *120*, 12910−12919.
(19) Hsu, H. F.; Dong, Y.; Shu, L.; Young, V. G., Jr.; Que, L., Jr. *J. Am. Chem. Soc.* **1999**, *121*, 5230−5237.
(20) Siegbahn, P. E. M. *Inorg. Chem.* **1999**, *38*, 2880−2889.

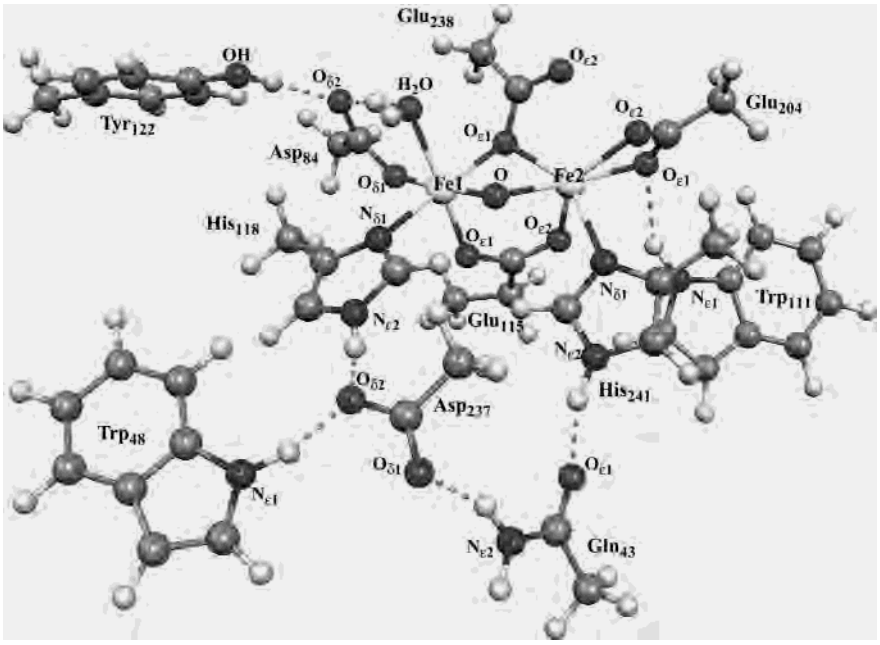

Figure 2. The representative model for the quantum cluster with a terminal H_2O $(H_2O)_t$. The model with a terminal hydroxide $(OH^-)_t$ is similar to this but without the hydrogen that has no H-bonding interaction.

tion methods.[21] By including some important second and third shell H-bonding partners, thereby significantly increasing the size of the active site quantum cluster for the Fe(III)-Fe(IV)(μ-O)(μ-OH) coordination geometry related to Siegbahn's, both high spin and intermediate site spin states have been examined, along with Fe(III) ↔ Fe(IV) valence interchange between Fe1 and Fe2. The lowest energy structure we obtained displays an Fe−Fe distance of 2.708 Å and intermediate spin AF-coupled Fe centers, corresponding to site spins for Fe1 and Fe2 of $S_{Fe1} = {}^3/_2$ and $S_{Fe2} = 1$, respectively. The intermediate spin AF-coupling conflicts with the high spin Fe sites indicated by Fe hyperfine spectra. Also, Mössbauer property calculations for three different spin-states of lowest energy for this model produce similar isomer shift values for Fe1 and Fe2. This contrasts with the experimental situation in which the two iron sites can be distinguished on the basis of their different isomer shift parameters. Further, for the AF-coupled $\{S_{Fe1} = {}^3/_2, S_{Fe2} = 1\}$ and $\{S_{Fe1} = 2, S_{Fe2} = {}^5/_2\}$ states with lowest energies, the calculated isomer shift and quadrupole splitting values of the Fe(IV) center are larger than the corresponding ones for the Fe(III) site, which is also inconsistent with the experimental data. On this basis, we therefore concluded that the model which contains two bidentate carboxylate groups and a bridging hydroxide is unlikely to be the core structure of X.[21]

In this second paper on proposed RNR-X type species, we present the results of our properties calculations on the model proposed by Burdi et al.[18] In Burdi's model, there is no bridging H_2O or OH^- since this would be inconsistent with observed anisotropic proton hyperfine spectra.[18] One of the oxygens of the carboxylate of Glu238 is thought to be present as a mono-oxygen bridge. A terminal H_2O or OH^- is also examined here. The initial structures were set up according to the RNR X-ray crystal structure[9] and then were geometry optimized to see if the carboxylate mono-oxygen bridge would remain and the short Fe−Fe = 2.5 Å distance could be reproduced.

2. Quantum Mechanical Cluster Model

The representative model with a terminal H_2O (or a terminal OH^- by deleting the proton which has no H-bonding interaction to Tyr122) is shown in Figure 2. As proposed by Burdi et al.,[18] there is a μ-oxo bridge and a terminal aqua ligand in the core structure of X and no bridging H_2O or OH. Since the μ-oxo bridge is between His118 and His241 in the active site of $R2_{ox}$(met), we retain this oxygen position in our model (O in Figure 2). There are two terminal H_2O ligands found in the crystal structure of $R2_{ox}$(met) (see Figure 1). One is between Asp84 and Glu204 and ligated to Fe2. According to our previous calculations,[21] when keeping the two carboxylates both bidentately ligated to the irons, this site prefers a bridging hydroxide rather than a terminal H_2O or terminal hydroxide. We therefore choose to keep the other terminal H_2O which is ligated to Fe1 in this model. Both terminal H_2O (denoted as $(H_2O)_t$) and terminal OH^- (as $(OH^-)_t$) forms are studied in this paper. Burdi et al.[18] also suggested that intermediate X contains one or two mono-oxygen bridges provided by the carboxylate oxygens of Glu115 and/or Glu238. Since the coordination mode of the carboxylate of Glu115 remains the same in both the diferrous and diferric centers, its bidentate coordination is kept in the model. Therefore only the carboxylate group of Glu238 is shifted to the position where $O_{\epsilon 1}$ is between the two iron sites and opposite to the bridging oxygen (O) (see Figure 2). Since the Tyr122 is not in the radical form in intermediate X, the H-bonding pattern between Tyr122 and Asp84 may reasonably be assumed to remain the same as that in the

(21) Han, W.-G.; Lovell, T.; Liu, T.; Noodleman, L. *Inorg. Chem.* **2003**, *42*, 2751−2758.

diferrous centers. The terminal H_2O or OH^- in our model is also H-bonded to $O_{\delta 2}$ of Asp84. For an improved representation of the structural and energetic effects of the protein environment, the main H-bonding residue side chains in the outer ligand shells are also included in the model. These residues are Trp111, Gln43, Asp237, and Trp48. The H-bonding interactions are (Trp111)$N_{\epsilon 1}H\cdots O_{\epsilon 1}$(Glu204), (Gln43)$O_{\epsilon 1}\cdots HN_{\epsilon 2}$(His241), (Asp237)$O_{\delta 2}\cdot\cdot HN_{\epsilon 2}$(His118), (Asp237)$O_{\delta 1}\cdot\cdot HN_{\epsilon 2}$(Gln43), and (Trp48)$N_{\epsilon 1}H\cdots O_{\delta 2}$(Asp237). The initial Cartesian coordinates of the model cluster are taken from chain A of the RNR X-ray crystal structure (PDB code:1XIK).[9] The orientation of the carboxylate group of Glu238 side chain was rearranged to a bridging monodentate ligating position. The bridging μ-oxo and terminal $H_2O(OH^-)$ were incorporated according to the positions described above. All side chain groups were extracted from the protein coordinates by breaking the $C_\beta-C_\alpha$ or $C_\gamma-C_\beta$ bonds. Then a linking hydrogen atom was added to fill the open valence of the ending carbon atom.[22]

3. Computational Methodology

All DFT spin-unrestricted calculations have been performed using the Amsterdam Density Functional (ADF, Version 2.3 and 2000.02) packages.[23−26] The parametrization of Vosko, Wilk, and Nusair (VWN)[27] was used for the local density approximation term, and the corrections of Perdew and Wang (PW91)[28] were used for the nonlocal exchange and correlation terms. During geometry optimizations in ADF2.3, basis set IV was applied for the two iron sites (uncontracted triple-ζ Slater-type orbitals (STO) for the 3s, 3p, 3d, and 4s valence orbitals along with a 4p polarization orbital) and basis set III for other atoms (double-ζ STOs for 2s, 2p valence orbitals of C, N, O augmented with a 3d polarization orbital, and double-ζ STO for 1s of H with a 2p polarization orbital). The inner core shells of C(1s), N(1s), O(1s), and Fe(1s,2s,2p) were treated by the frozen core approximation. For Mössbauer parameter and hyperfine coupling calculations, the electronic densities were obtained by single-point energy calculations on the optimized geometries using basis set IV in ADF2000.02 for all atoms (triple-ζ STOs for 2s, 2p valence orbitals of C, N, O augmented with a 3d polarization orbital, and triple-ζ STO for 1s of H with a 2p polarization orbital), and no frozen core approximation was applied. The accuracy parameter for the numerical integration grid was set to 4.0.

Experimentally, X is assigned as an Fe(III)Fe(IV) $S_{total} = {}^1/_2$ ground state, and the two Fe sites are high spin and antiferromagnetically (AF) coupled.[3] We therefore performed geometry optimizations on two kinds of spin states of $\{S_1 = {}^5/_2, S_2 = -2\}$ and $\{S_1 = -2, S_2 = {}^5/_2\}$, for the $(H_2O)_t$ and $(OH^-)_t$ clusters. (Note: total spin quantum numbers cannot be negative. We use the negative sign to simply denote the AF coupling arrangement.)

Usually the AF spin-coupled state cannot be obtained directly from the normal DFT calculations in ADF. As in previous work, we represent the AF spin-coupled state in DFT by a "broken-symmetry" state, where a spin-unrestricted determinant is constructed in which one of the Fe site adopts spin-up electrons and the other site has spin-down electrons.[29−33] To obtain this broken-symmetry solution, we first construct a ferromagnetically (F) spin-coupled ($S_{max} = S_{total} = {}^9/_2$) determinant, where the spins on both irons are aligned in a parallel fashion. Then we rotate the spin vector located on either atom Fe1 or atom Fe2 by interchanging the α and β fit density blocks on the site Fe1 or Fe2 from the output file TAPE21 created by this F-coupled calculation in ADF. Using the modified TAPE21 as a restart file and reading the starting spin density from there, we then obtain the expected broken-symmetry state through single-point energy calculation or geometry optimization.

More detailed information for obtaining isomer shift (δ) and quadrupole splitting (QS) properties can be found in ref 34. The correlation between isomer shifts δ and Fe nuclear densities $\rho(0)$ is given by

$$\delta = \alpha(\rho(0) - 11884.0) + C \qquad (1)$$

where $\alpha = -0.664$, and $C = 0.478$ were obtained from a linear correlation between measured isomer shifts and calculated electron densities for a series of 15 dinuclear plus 6 polar mononuclear iron complexes.[34] The best fit equation gave a correlation coefficient ($r = -0.94$) with a standard deviation of 0.11 mm/s.

For predicting the ligand ^{1}H proton and ^{17}O hyperfine coupling constants, we performed both simple estimations (see Appendix) and more accurate **A** tensor calculations based on computed electronic spin densities using ADF2000.02.[24−26] In the estimations, the ligand ^{1}H hyperfine coupling constants were determined by the distance between the proton and the closest Fe site; the ^{17}O isotropic hyperfine coupling constants were calculated using Mulliken valence O(2s) spin populations. The **A** tensors obtained by ADF calculations were based on the assumption that there was only one unpaired electron in the system. For the present system with high spin AF coupled sites, we therefore need to rescale the ADF-obtained **A** tensors by the spin coupling factors $K_A/2S_A$ for Fe(III) ($K_A = {}^7/_3$, $S_A = {}^5/_2$) and $K_B/2S_B$ for Fe(IV) ($K_B = -{}^4/_3$, $S_B = 2$).[35] For the terminal OH^- or H_2O group, the coupling factors are determined by whether Fe1 is a ferric or ferrous center. For the

(22) Han, W.-G.; Tajkhorshid, E.; Suhai, S. *J. Biol. Struct. Dyn*. **1999**, *16*, 1019−1032.
(23) (a) *ADF 2.3.0*; Theoretical Chemistry, Vrije Universiteit: Amsterdam. (b) Baerends, E. J.; Ellis, D. E.; Ros, P. *Chem. Phys*. **1973**, *2*, 41−59. (c) te Velde, G.; Baerends, E. J. *J. Comput. Phys*. **1992**, *99*, 84−98. (d) Guerra, C. F.; Visser, O.; Snijders, J. G.; te Velde, G.; Baerends, E. J. In *Methods and Techniques for Computational Chemistry*; Clementi, E., Corongiu, G., Eds; STEF: Cagliari, 1995; p 305.
(24) *ADF 2000.02*; Theoretical Chemistry, Vrije Universiteit: Amsterdam.
(25) van Lenthe, E.; van der Avoird, A.; Wormer, P. E. S. *J. Chem. Phys*. **1998**, *108*, 4783−4796.
(26) Te Velde, G.; Bickelhaupt, F. M.; Baerends, E. J.; Guerra, C. F.; van Gisbergen, S. J. A.; Snijders, J. G.; Ziegler, T. *J. Comput. Chem.* **2001**, *22*, 931−967.
(27) Vosko, S. H.; Wilk, L.; Nusair, M. *Can. J. Phys*. **1980**, *58*, 1200−1211.
(28) Perdew, J. P.; Chekavry, J. A.; Vosko, S. H.; Jackson, K. A.; Perderson, M. R.; Singh, D. J.; Fioihais, C. *Phys. Rev. B* **1992**, *46*, 6671−6687.
(29) Noodleman, L.; Case, D. A. *Adv. Inorg. Chem*. **1992**, *38*, 423−470.
(30) Mouesca, J.-M.; Chen, J. L.; Noodleman, L.; Bashford, D.; Case, D. A. *J. Am. Chem. Soc*. **1994**, *116*, 11898−11914.
(31) Zhao, X. G.; Richardson, W. H.; Chen, J.-L.; Li, J.; Noodleman, L.; Tsai, H.-L.; Hendrickson, D. N. *Inorg. Chem*. **1997**, *36*, 1198−1217.
(32) Li, J.; Noodleman, L. In *Spectroscopic Methods in Bioinorganic Chemistry*; Solomon, E. I., Hodgson, K. O., Eds.; ACS Symposium Series 692; American Chemical Society: Washington, DC, 1998; Chapter 9, pp 179−195.
(33) Case, D. A.; Noodleman, L.; Li, J. In *Metal−Ligand Interactions in Chemistry, Physics and Biology*; Russo, N., Salahub, D. R., Eds.; Kluwer Academic Publishers: Dordrecht, The Netherlands, 2000; pp 19−47.
(34) (a) Lovell, T.; Han, W.-G.; Liu, T.; Noodleman, L. *J. Am. Chem. Soc*. **2002**, *124*, 5890−5894. (b) Liu, T.; Lovell, T.; Han, W.-G.; Noodleman, L. *Inorg. Chem*. **2003**, *42*, 5244−5251.
(35) Noodleman, L.; Chen, J.-L.; Case, D. A.; Giori, C.; Rius, G.; Mouesca, J.-M.; Lamotte, B. In *Nuclear Magnetic Resonance of Paramagnetic Macromolecules*; Kluwer Academic Publishers: The Netherlands, 1995; pp 339−367.

bridging oxo, the coupling factor was chosen depending on whether the dominant coupling is due to Fe(III) or Fe(IV).

To examine whether a terminal H_2O or terminal hydroxide is favored in this model cluster, we need to calculate the pK_a values for the $-H_2O$ ligand (L) forms. The detailed procedure for pK_a calculations can be found from our previous work.[36−38] First we used a modified version of CHELPG code[39] to fit the point charges from the molecular electrostatic potentials calculated by ADF. Then for solvation energy calculations, we used the MEAD (Macroscopic Electrostatics with Atomic Detail) program suite developed by Bashford, to solve the Poisson−Boltzmann equation using a finite-difference method.[40,41] The solute is represented by a set of atomic charges and Born radii. The dielectric constant in the solute region is set to $\epsilon = 1.0$. Three kinds of conditions are considered for the solvent environment. The first is to treat the solvent as water, that is a continuous dielectric medium with $\epsilon = 80.0$. The second is to use $\epsilon = 4$ for the medium, representing the cluster within a low dielectric protein environment. The third is to consider both the protein field and reaction field.[36,38] The PARSE[42] charges and radii were assigned to atoms in the protein field. Again the dielectric constant in the protein region is set to 4.0, and that in the solvent water region is set to 80.0. Finally for the following process

$$L(H_2O) \rightarrow L(OH^-) + H^+ \quad (2)$$

the pK_a value for the L(H_2O) cluster can be calculated by

$$1.37pK_a = \{E[L(OH^-)] + E[H^+] - E[L(H_2O)] + E_{corr}\} + \{G_{sol}[L(OH^-)] - G_{sol}[L(H_2O)]\} - 268.26 = PA + \Delta G(\text{deproton}) - 268.26 \quad (3)$$

where E[L(OH^-)] and E[L(H_2O)] represent the gas-phase energies for the active site clusters with ligand $-OH^-$ and $-H_2O$, respectively; $E[H^+] = 12.6523$ eV is the calculated ionization energy of a spin restricted H atom obtained from DFT calculation; E_{corr} is a correction term to the proton affinity PA, including an estimate of the zero point energy ($\Delta ZPE = -7.7$ kcal/mol)[36] and $^5/_2RT$ work term. The quantity −268.26 kcal/mol comes from the sum of the solvation free energy of a proton (−260.5 kcal/mol)[43,44] (using the estimated value of Noyes), and the translation entropy contribution to the gas-phase free energy of a proton ($-T\Delta S_{gas}(H^+) = -7.76$ kcal/mol at 298 K and 1 atm pressure).[44] G_{sol} represents solvation energy, and it contains both the reaction and protein field energies in the third case.

4. Results and Discussion

Geometry optimizations for two kinds of spin state of $\{S_1 = {}^5/_2, S_2 = -2\}$ and $\{S_1 = -2, S_2 = {}^5/_2\}$ have been obtained for the $(OH^-)_t$ and $(H_2O)_t$ cluster models. The spin S_1 corresponds to that on site Fe1 nearer to Tyr122 (see Figure 2). Mössbauer properties, ^{1}H proton hyperfine couplings on $(OH^-)_t$ or $(H_2O)_t$ clusters, and ^{17}O couplings are then calculated at the optimized geometries. The bond lengths of the core structure, net spin populations, broken-symmetry state energies (E_{BS}), isomer shift (δ) values, and quadrupole splitting (QS) values for the clusters are given in Table 1. The estimations for ^{1}H proton hyperfine and ^{17}O isotropic couplings using the simple methods in Appendix are given in Table 2. The DFT calculated ^{1}H proton and ^{17}O hyperfine couplings (rescaled by the spin coupling factors) are given in Table 3.

Table 1. Geometries (Å), Net Spin Populations, Broken-Symmetry State Energies (E_{BS}) (eV), Isomer Shift δ Values (mm/s), and Quadrupole Splitting (QS) Values (mm/s) for the Model Clusters with Terminal Hydroxide $(OH^-)_t$ and Terminal H_2O $(H_2O)_t$ in Different Spin States

	$(OH^-)_t$		$(H_2O)_t$	
	$S_1 = {}^5/_2$ $S_2 = -2$	$S_1 = -2$ $S_2 = {}^5/_2$	$S_1 = {}^5/_2$ $S_2 = -2$	$S_1 = -2$ $S_2 = {}^5/_2$
	Geometry			
Fe1−Fe2	2.973	2.970	2.911	3.105
Fe1−O	1.773	1.729	1.823	1.734
Fe2−O	1.777	1.846	1.742	1.821
Fe1−$O_{\epsilon1}$(Glu238)	2.534	2.552	2.350	1.942
Fe2−$O_{\epsilon1}$(Glu238)	1.912	1.985	2.001	3.126
Fe2−$O_{\epsilon2}$(Glu238)	3.321	3.441	3.397	2.101
Fe1−O(OH^- or H_2O)	1.790	1.781	2.114	2.255
Fe1−$O_{\delta1}$(Asp84)	2.013	1.973	2.051	1.981
Fe1−$N_{\delta1}$(His118)	2.175	2.181	2.158	2.040
Fe1−$O_{\epsilon1}$(Glu115)	2.080	2.032	2.027	2.093
Fe2−$O_{\epsilon1}$(Glu204)	3.183	2.237	2.046	2.130
Fe2−$O_{\epsilon2}$(Glu204)	1.896	2.067	2.161	2.198
Fe2−$N_{\delta1}$(His241)	2.046	2.239	2.140	2.151
Fe2−$O_{\epsilon2}$(Glu115)	2.058	2.076	2.096	2.044
O(Tyr122)···$O_{\delta2}$	2.701	2.701	2.710	2.736
$O_{\delta2}$···O(OH^- or H_2O)	2.706	2.704	2.553	2.576
	Net Spin Population[a]			
Fe1	−3.27	−2.91	3.67	−2.79
Fe2	−2.70	3.83	−3.19	3.70
O	0.06	−0.10	−0.06	−0.04
O(OH^- or H_2O)	0.32	−0.27	0.07	−0.07
$O_{\epsilon1}$(Glu238)	0.01	0.12	−0.02	−0.01
$O_{\epsilon2}$(Glu115)	−0.12	0.09	−0.09	0.11
$N_{\delta1}$(His118)	0.11	−0.11	0.08	0.00
$O_{\epsilon2}$(Glu204)	−0.02	0.15	−0.13	0.14
E_{BS}	−783.6290	−783.9357	−784.3001	−784.6581
$\delta(Fe_1)$[b]	0.17	0.05		0.33
$\delta(Fe_2)$[b]	0.34	0.65		0.72
$QS(Fe_1)$[c]	−0.63	0.29		1.10
$QS(Fe_2)$[c]	2.0	−0.55		−1.10

[a] The net spins on the ligated atoms which are larger than 0.10 in one of the states are given here. [b] The experimental isomer shift values are 0.56 (for Fe(III)) and 0.26 (for Fe(IV)) mm/s. [c] The experimental quadrupole splitting values are −0.90 (for Fe(III)) and −0.60 (for Fe(IV)) mm/s.

4.1. $(OH^-)_t$ Clusters. The optimized structure for the spin state $\{S_1 = -2, S_2 = {}^5/_2\}$ is of lower energy (by 7.1 kcal/mol for the broken-symmetry energy) than the $\{S_1 = {}^5/_2, S_2 = -2\}$ state. Therefore, site Fe1 with a hydroxide ligand is the Fe(IV) center. During the geometry optimizations, the oxygen $O_{\epsilon1}$ of Glu238 moved much closer to Fe2 than to Fe1. The distance between the $O_{\epsilon1}$(Glu238) and Fe1 is more than 2.5 Å in both the Fe1(III)Fe2(IV) and Fe1(IV)Fe2(III) states. The Fe1−Fe2 distances in the two structures are quite similar (2.973 and 2.970 Å) and are much longer than the

(36) (a) Richardson, W. H.; Peng, C.; Bashford, D.; Noodleman, L.; Case, D. A. *Int. J. Quantum Chem*. **1997**, *61*, 207−217. (b) Li, J.; Fisher, C. L.; Konecny, R.; Bashford, D.; Noodleman, L. *Inorg. Chem*. **1999**, *38*, 929−939.
(37) Huang, H.; Han, W.-G.; Noodleman, L.; Grynszpan, F. *Bioorg. Med. Chem*. **2001**, *9*, 3185−3195.
(38) Han, W.-G.; Lovell, T.; Noodleman, L. *Inorg. Chem*. **2002**, *41*, 205−218.
(39) Breneman, C. M.; Wiberg, K. B. *J. Comput. Chem*. **1990**, *11*, 361−373.
(40) Bashford, D.; Gerwert, K. *J. Mol. Biol*. **1992**, *224*, 473−486.
(41) Bashford, D. In *Scientific Computing in Object-Oriented Parallel Environments*; Ishikawa, Y., Oldehoeft, R. R., Reynders, J. V. W., Tholburn, M., Eds.; Lecture Notes in Computer Science; Springer: Berlin, 1997; Vol. 1343, p 233.
(42) Sitkoff, D.; Sharp, K. A.; Honig, B. *J. Phys. Chem*. **1994**, *98*, 1978.
(43) (a) Noyes, R. M. *J. Am. Chem. Soc*. **1962**, *84*, 512−522. (b) Reiss, H.; Heller, A. *J. Phys. Chem*. **1985**, *89*, 4207.
(44) Tawa, G. J.; Topol, I. A.; Burt, S. K.; Caldwell, R. A.; Rashin, A. A. *J. Chem. Phys*. **1998**, *109*, 4852−4863.

Table 2. Estimates of Ligand Hyperfine Coupling Constants (MHz)[a]

	calculations				
	$(OH^-)_t$		$(H_2O)_t$		
property	$S_1 = 5/2$, $S_2 = -2$	$S_1 = -2$, $S_2 = 5/2$	$S_1 = 5/2$, $S_2 = -2$	$S_1 = -2$, $S_2 = 5/2$	experiment
r(Fe1−H)[b]	2.27	2.26	2.53, 2.60	2.56, 2.71	
A_3^{aniso}(H)[c]	29	−17	21, 19	−12, −10	20.5, 17.6[h]
$A^{iso}(O_{br})$[d]	−6	+3	−2	−5	15.3[i]
$A^{iso}(O_t)$[e]	−22	−12	+10	+6	23.8[i]
2s-net-spin(O_{br})[f]	0.0024	0.0016	0.0013	0.0026	
2s-net-spin(O_t)[g]	0.009	−0.007	0.0042	−0.0033	

[a] The estimation methods are given in the Appendix. [b] The distances (Å) between Fe1 and the protons on the terminal OH^- or H_2O groups. [c] Proton hyperfine coupling constants (MHz). A_3^{aniso}(H) is the largest principal value of the axial dipolar tensor. [d] ^{17}O isotropic hyperfine coupling constants (MHz) for the bridging oxygen atom. [e] ^{17}O isotropic hyperfine coupling constants (MHz) for the oxygen atom of the terminal OH^- or H_2O. [f] The net spin population for the 2s orbital of the bridging oxygen atom. [g] The net spin population for the 2s orbital of oxygen atom of the terminal OH^- or H_2O. [h] From ref 16. [i] From ref 18.

Table 3. DFT-Calculated Ligand Hyperfine Coupling Constants (MHz) Compared with Experimental Results[a]

	calculations			
	$(OH^-)_t$		$(H_2O)_t$	
property	$S_1 = 5/2$, $S_2 = -2$	$S_1 = -2$, $S_2 = 5/2$	$S_1 = -2$, $S_2 = 5/2$	experiment[b]
Proton Hyperfine Coupling Constants				
A_1^{aniso}(H)	−14.0	5.9	2.6, 1.9	−10.25, −8.8
A_2^{aniso}(H)	−9.4	7.8	6.1, 6.3	−10.25, −8.8
A_3^{aniso}(H)	23.4	−13.7	−8.7, −8.2	20.5, 17.6
A^{iso}(H)	5.5	−2.5	1.6, 0.8	
^{17}O Hyperfine Coupling Constants				
$A_1(O_{br})$	−2.2	−0.5	−1.6	0
$A_2(O_{br})$	−9.2	−8.1	−6.7	22.5
$A_3(O_{br})$	−24.9	−19.9	−20.9	23.5
$A^{iso}(O_{br})$[c]	−12.1	−9.5	−9.8	15.3
$A_1^{aniso}(O_{br})$	9.9	9.0	8.1	−15.3
$A_2^{aniso}(O_{br})$	2.9	1.4	3.0	7.2
$A_3^{aniso}(O_{br})$	−12.8	−10.4	−11.1	8.2
$A_1(O_t)$	2.3	−5.7	8.8	17
$A_2(O_t)$	−8.9	−1.1	9.0	20.5
$A_3(O_t)$	−46.6	32.1	24.3	34.0
$A^{iso}(O_t)$	−17.7	8.4	14.0	23.8
$A_1^{aniso}(O_t)$	20.0	−14.1	−5.2	−6.8
$A_2^{aniso}(O_t)$	8.8	−9.5	−5.0	−3.3
$A_3^{aniso}(O_t)$	−28.8	23.6	10.3	10.2

[a] DFT-calculated tensors were rescaled by the spin coupling factors (see text). [b] Proton hyperfine coupling constants are taken from ref 16. The principal values of the ^{17}O hyperfine coupling constants for the bridging (br) and terminal (t) oxygen atoms are taken from ref 18. For the experimental tensors, which are based on parameter fits to the observed ENDOR spectra, the relative signs of the 3 principal values were determined, but the absolute signs are not known. Therefore, at present, the overall tensors may be ±1 times the values given. [c] The spin coupling model we have used assumes that a dominant spin vector can be identified. This is more problematic for the bridging O than for the terminal OH^- or H_2O ligands.

2.5 Å indicated from analysis of EXAFS measurements. The 2.9 Å value is also substantially larger than 2.76 Å from our previously calculated model.[21] In the Fe1(IV)Fe2(III) state, both the oxygen atoms $O_{\epsilon 1}$ and $O_{\epsilon 2}$ in the carboxylate group of the terminal Glu204 are coordinated to Fe2 with the bonding distances of 2.237 and 2.067 Å, respectively. Atom $O_{\epsilon 1}$ of Glu204 is also H-bonding to the $N_{\epsilon 1}H$ group of Trp111 with $O_{\epsilon 1}\cdots H$ distance of 1.970 Å. By contrast, for the Fe1(III)Fe2(IV) state, only $O_{\epsilon 2}$ of Glu204 is ligated to site Fe2 with a shorter distance of 1.869 Å, and $O_{\epsilon 1}$ is much farther from Fe2 (the distance of Fe2-$O_{\epsilon 1}$ is 3.183 Å) but still H-bonding to the $N_{\epsilon 1}H$ group of Trp111 with the $O_{\epsilon 1}\cdots H$ distance of 1.931 Å. So, the nature of the spin and oxidation state of Fe2 has a major effect on the coordination mode of Glu204-O_ϵ atoms.

The net spin populations are the main indication of the high spin or intermediate spin character of the Fe sites. In the ideal ionic limit, the net unpaired spin populations are 5 and 4 for the high spin Fe(III) (five d-electrons) and Fe(IV) (four d-electrons) sites, respectively. The absolute calculated net spins in Table 1 are smaller (by about $1e^-$) than the ionic limit, indicative of substantial Fe−ligand covalency and consistent with previous results in related complexes including $R2_{ox}$(met).[5] The opposite signs for the spin densities of Fe1 and Fe2 confirm the AF-coupling. Experimentally, it has been observed that there is significant spin delocalization onto the oxygen ligand(s).[3] The net spins on the bridging O atom and the assumed mono-oxygen bridge of atom $O_{\epsilon 1}$ of Glu238 are small in the Fe1(III)Fe2(IV) state, while in the Fe1(IV)Fe2(III) state, there are larger amounts (around 0.1) of spin delocalization onto the oxygen atoms, including the bridging oxygen, O(OH^-), $O_{\epsilon 1}$(Glu238), $O_{\epsilon 2}$(Glu115), and $O_{\epsilon 2}$(Glu204).

Further we performed Mössbauer property calculations on the two broken-symmetry state optimized structures. The experimental isomer shifts (δ) for Fe(III) and Fe(IV) sites are 0.56 and 0.26 mm/s, respectively. Corresponding quadrupole splitting (QS) values are −0.90 and −0.60 mm/s. For the Fe1(III)Fe2(IV) state, our calculated isomer shift values are 0.17 and 0.34 mm/s, and the quadrupole splitting values are −0.63 and 2.0 mm/s, for Fe1(III) and Fe2(IV), respectively (see Table 1). The calculated absolute isomer shift and quadrupole splitting values for site Fe1(III) are smaller than the corresponding ones for the Fe2(IV) site, which is in contrast with the measured results that the values of δ and QS for Fe(III) site are larger than for Fe(IV). For the Fe1(IV)Fe2(III) state, the calculated isomer shifts are δ(Fe1) = 0.05 mm/s and δ(Fe2) = 0.65 mm/s, and the quadrupole splittings are QS(Fe1) = 0.29 and QS(Fe2) = −0.55 mm/s. The ordering of these values and their magnitudes, while showing far from perfect agreement (δ(Fe1) is too small), is consistent with the experimental values; i.e., the calculated absolute values of δ and QS for site Fe(III) are larger than the corresponding ones for site Fe(IV). In this model, both the isomer shift and quadrupole splitting values for the two iron sites are distinct from each other, so that one can clearly distinguish the Fe(III) and Fe(IV) centers. Our calculated Fe(IV) site isomer shift of 0.05 mm/s is much closer to that of AF coupled, valence localized $[L_2Fe(III)Fe(IV)O_2]^{3+}$ synthetic complexes (where L = 6-Me-tpa or 6-Me_3-tpa) having δ[Fe(IV)] = 0.08, 0.10 mm/s smaller than the more "covalent" Fe(IV) site in RNR-X where δ = 0.26 mm/s.[45]

Very recently, we performed Mössbauer property calculations on another Fe(III)−O−Fe(IV) model which has a

(45) Que, L., Jr.; Tolman, W. B. *Angew. Chem., Int. Ed.* **2002**, *41*, 1114−1137.

bridging hydroxide and two bidentate bridging carboxylate groups from Glu115 and Glu238. Both isomer shift and quadrupole splitting values for the two iron sites of the $\{S_1 = -2, S_2 = {}^5/_2\}$ (Fe1(IV)Fe2(III)) state of that model are very close (with δ(Fe1) = 0.33, δ(Fe2) = 0.29, QS(Fe1) = −1.90 and QS(Fe2) = 1.70 mm/s).[21] On the basis of these calculations, it appears the model with a terminal hydroxide and Fe1(IV)Fe2(III) oxidation states yields a better description for the Mössbauer properties of the RNR intermediate X.

4.2. $(H_2O)_t$ Clusters. As was found for the $(OH^-)_t$ clusters, the structure with a terminal H_2O for the spin state of $\{S_1 = -2, S_2 = {}^5/_2\}$ also has a lower energy (by 8.3 kcal/mol in broken-symmetry energy) than the $\{S_1 = {}^5/_2, S_2 = -2\}$ state. The Fe1−Fe2 distances in the two spin states are again longer than 2.9 Å. The terminal H_2O is predicted to be closer (by 0.141 Å) to the Fe1 center when Fe1 is the ferric site. Both oxygen atoms $O_{\epsilon 1}$ and $O_{\epsilon 2}$ in the carboxylate group of Glu204 are ligated to the Fe2 site, and the bridging oxygen O is closer to the Fe(IV) center in both $(H_2O)_t$ structures. In the $\{S_1 = {}^5/_2, S_2 = -2\}$ state, the bridging $O_{\epsilon 1}$ of Glu238 is closer by 0.35 Å to the Fe2 site, and the distance for Fe2−$O_{\epsilon 2}$(Glu238) (3.397 Å) is very long. For the $\{S_1 = -2, S_2 = {}^5/_2\}$ state, $O_{\epsilon 1}$ of Glu238 is bonded to the Fe1 site alone, while $O_{\epsilon 2}$ of Glu238 is bonded to Fe2 at a distance of 2.101 Å.

Since the $\{S_1 = -2, S_2 = {}^5/_2\}$ $(H_2O)_t$ cluster is much lower in energy than the $\{S_1 = {}^5/_2, S_2 = -2\}$ cluster, we performed Mössbauer property calculations only on the former. The isomer shift values δ(Fe1) = 0.33 and δ(Fe2) = 0.72 mm/s appear reasonably consistent with the experimental data of δ(Fe(IV)) = 0.26 and δ(Fe(III)) = 0.56 mm/s. However, the absolute calculated quadrupole splitting values are the same (1.10 mm/s) for the two iron sites, which is inconsistent with the experimental values of QS(Fe(IV)) = −0.60, QS(Fe(III)) = −0.90 mm/s.

Some more global observations can be made about the Mössbauer isomer shifts we have calculated. Taking a reasonable Fe−L coordination cutoff of Fe−L < 2.3 Å, the first, second, and fourth complexes in Table 1 have Fe(III) coordination numbers of 5, 6, and 6, respectively, and corresponding calculated isomer shifts of 0.17, 0.65, and 0.72 mm/s. Typical variation for experimental high spin Fe(III) ranges from 0.27 to 0.64 mm/s (corrected to 4 K for the second order Doppler shift) on going from tetrahedral to octahedral coordination in an oxygen rich environment,[12] and six coordinate diferric peroxo complexes can have isomer shifts of 0.66 mm/s.[46] Therefore, the same general trend with increasing coordination number is shown for Fe(III), and these calculations match the experimental range to within about one standard deviation (based on our prior linear correlation, SD = 0.11 mm/s for synthetic complexes). For high-spin Fe(IV) in synthetic iron dimer complexes and proteins, experimental isomer shifts vary from 0.08 to 0.26 mm/s, which is similar to the range 0.05−0.34 mm/s,[47] found in our calculations in Table 1, and in our previous calculations for the Fe(IV) dimer in our models of the high-valent intermediate Q in methane monooxygenase.[34] Notably, for complex **1** (OH^-, $S_1 = {}^5/_2$, $S_2 = -2$) which has a higher calculated isomer shift for the Fe(IV) site compared to the Fe(III) site, both Fe sites are strongly coordinated to the bridging oxo group and 5 coordinate, and the spin population on Fe(III) is comparatively low (3.3) compared to other Fe(III) sites (3.7−3.8), suggesting some "mixed-valent" character involving Fe(IV) (and perhaps also some fractional intermediate spin Fe(III) character). (See Fe(III) and Fe(IV) range in Gütlich and Ensling.[48])

One cannot compare the absolute energies between the $(H_2O)_t$ and $(OH^-)_t$ clusters because the clusters have different numbers of protons. We then calculated the pK_a values for the $-H_2O$ ligand forms in order to compare the relative stability between the $(H_2O)_t$ and $(OH^-)_t$ cluster forms. As described in section 3, three kinds of solvation environment are considered here. The first is a continuum dielectric medium with $\epsilon = 80$ (water), the second is a medium with smaller dielectric constant $\epsilon = 4$ (appropriate for a protein environment), and the third is to consider both the protein and water environments with $\epsilon = 4$ for the protein region (plus point charges in atomic positions) and $\epsilon = 80$ for outer area. The three pK_a values for the $\{S_1 = {}^5/_2, S_2 = -2\}$ state $(H_2O)_t$ cluster are 0.26, 6.80, and 5.71, and for the lower energy $\{S_1 = -2, S_2 = {}^5/_2\}$ $(H_2O)_t$ state these pK_a values are 2.41, 8.39, and 4.55. It is obvious that the pK_a values vary with the environment. The $(OH^-)_t$ cluster form is favored in the very polar environment with $\epsilon = 80$. The pK_a values are increased to about 7 and 8 when using $\epsilon = 4$, and the $(H_2O)_t$ and $(OH^-)_t$ forms may coexist in this environment. When both the protein and reaction fields are considered, the pK_a values are between the two extremes and are still smaller than 7. Therefore, the $(OH^-)_t$ form of this model cluster is energetically preferred to the corresponding $(H_2O)_t$ cluster within the protein and water environment. Overall, from the energy, pK_a, and Mössbauer properties analysis, the $\{S_1 = -2, S_2 = {}^5/_2\}$ state $(OH^-)_t$ cluster gives a better description than the other three possibilities for the core structure of RNR intermediate X. Its Fe−Fe distance (2.970 Å), however, is much longer than the EXAFS value of 2.5 Å. The atom $O_{\epsilon 1}$ of Glu238, which is supposed to be a bridging oxygen, actually binds to Fe2 (1.985 Å) and consequently is very far from Fe1 (2.55 Å).

4.3. Ligand Hyperfine Coupling. The estimates (see Appendix) of the ^{1}H proton hyperfine couplings on $(OH^-)_t$ or $(H_2O)_t$ clusters and ^{17}O isotropic couplings are given in Table 2, and the more accurate DFT-calculated ^{1}H proton and ^{17}O hyperfine couplings (rescaled by the spin coupling factors) are given in Table 3 and compared with experimental values for RNR-X.[16,18] Comparing the two methods, the simple estimates predict reasonable values for the largest

(46) Kim, K.; Lippard, S. J. *J. Am. Chem. Soc.* **1996**, *118*, 4914−4915.

(47) Que, L., Jr.; Dong, Y.; Shu, L.; Wilkinson, E. C. In *Spectroscopic Methods in Bioinorganic Chemistry*; Solomon, E. I., Hodgson, K. O., Eds.; ACS Symposium Series 692; American Chemical Society: Washington, DC, 1998; Chapter 22, pp 374−386.

(48) Gütlich, P.; Ensling, J. In *Inorganic Electronic Structure and Spectroscopy*; Soloman, E. I., Lever, A. B. P., Eds.; John Wiley & Sons: New York, 1999; pp 161−211.

axial dipolar tensor of the ^{1}H proton hyperfine couplings, but all are somewhat larger than the corresponding DFT-calculated values. These higher values for the simple estimates are caused by the assumption of purely localized spin density at Fe(III) or Fe(IV), and the use of the nearer Fe to the proton as the sole source of spin density (see ref 16 and our Appendix for more details). The calculated DFT spin density is more delocalized (see Table 1). Also the ^{17}O isotropic couplings for the bridging (br) oxo predicted by the Mulliken valence spin population estimates are too small comparing with the DFT-calculated and the experimental results.

Comparing the explicit DFT-calculated ^{1}H proton and ^{17}O hyperfine couplings with the experiments, none of the three models reproduce all the experimental values. However, the first cluster, that is $(OH^-)_t$ in the ($S_1 = {}^5/_2$, $S_2 = -2$) state, is the best in reproducing the overall hyperfine couplings. This model gives reasonable values for ^{1}H proton anisotropic hyperfine couplings ($A_{1,2,3}^{aniso}$(H)) and ^{17}O isotropic ($A^{iso}(O_{br})$) coupling for the bridging oxo, and the ^{17}O isotropic ($A^{iso}(O_t)$) coupling constant for the terminal oxygen. This seems to support the assumption that the terminal oxygen group is ligated to the Fe(III) site in RNR-X.[16] Though the second model ($(OH^-)_t$ in ($S_1 = {}^5/_2$, $S_2 = -2$) state) gives the best Mössbauer parameters among these three models, it shows very small absolute values for the hyperfine couplings of A_3^{aniso}(H), $A^{iso}(O_{br})$, and $A^{iso}(O_t)$, and a very large value for $A_3^{aniso}(O_t)$, comparing with the corresponding experimental data.

Conclusions

On the basis of experimental observations,[16,17] Burdi et al.[18] proposed a structure for the diiron center of RNR intermediate X, which contains a single oxo bridge, one terminal aqua ligand bound to Fe(III), and one or two additional mono-oxygen bridges provided by the carboxylate oxygens of Glu115 and Glu238. In this paper, we have developed a model for the structure of X by following the proposal of Burdi et al., such that the bidentate coordination of Glu115 is maintained in our model. Only the carboxylate group of Glu238 was reoriented to a monodentate position with $O_{\epsilon 1}$ bridging between the two iron sites (see Figure 2). The possibilities that H_2O and hydroxide are terminal ligands bound to Fe1, defined as the Fe closer to Tyr122, are considered.

On the basis of Mössbauer and Q-band ENDOR spectroscopy,[3] we have geometry optimized model clusters containing iron centers that are high spin Fe(III) ($S = {}^5/_2$) and high spin Fe(IV) ($S = 2$) sites that antiferromagnetically couple to give an $S_{total} = {}^1/_2$ ground state. For both the $(H_2O)_t$ and $(OH^-)_t$ cases, the $\{S_1 = -2, S_2 = {}^5/_2\}$ state is lower in energy than the corresponding $\{S_1 = {}^5/_2, S_2 = -2\}$ state. In the lower energy state, the OH^- or H_2O is coordinated to the Fe(IV) site.

From the energy and pK_a analysis, the $\{S_1 = -2, S_2 = {}^5/_2\}$ state of the $(OH^-)_t$ cluster is the most stable structure among the four clusters studied here, and its calculated isomer shift and quadrupole splitting values are also in the best agreement with the experimental values. However, the DFT-calculated ^{1}H proton and ^{17}O hyperfine coupling constants on this model are not in agreement with the experiments. This state is also inconsistent with the proposal that Fe1 (the site closer to Tyr122) of X is in the +3 oxidation state, which was proposed on the basis of Bollinger's selective ^{57}Fe incorporation experiments and evaluation of which site is Fe1 based on the diferric Mössbauer spectrum.[49] Further, the Fe−Fe distances are all longer than 2.9 Å in the $(H_2O)_t$ and $(OH^-)_t$ model clusters, a feature inconsistent with the very short distance of 2.5 Å predicted by the EXAFS measurements. EXAFS is often quite accurate for Fe−ligand and Fe−Fe distances; however, errors of up to 0.2 Å compared to subsequent X-ray structures have been found for Fe−Fe distances in some synthetic systems.[19] Even by assigning a 0.2 Å error bar to the EXAFS datum, the 2.97 Å Fe−Fe distance still seems too long. The atom $O_{\epsilon 1}$ of Glu238, which is proposed to function as a bridging oxygen, is always much closer to one of the Fe sites in the four complexes and does not act as a mono-oxygen bridge to shorten the Fe−Fe distance. By considering all these factors, the models studied here are still unlikely to be representative of the core structures of RNR intermediate X.

It is well-known that there are two crystallized synthetic diiron systems which produce short Fe−Fe distances. One is the $[Fe(III)Fe(IV)(\mu\text{-}O)_2(5\text{-}Et_3\text{-}TPA)_2](ClO_4)_3$ cluster (with $S_1 = {}^1/_2$, $S_2 = 1$, and $S_{total} = {}^3/_2$), which contains an $Fe_2(\mu\text{-}O)_2$ core, that results in an Fe−Fe distance of 2.683 Å.[19,50−52] Our previous Fe(III)−O−Fe(IV) model,[21] which contains two bidentate bridging carboxylates from Glu115 and Glu238, and a bridging hydroxide, also yields a short Fe1−Fe2 distance of 2.561 Å for the mixed valent $S_{total} = {}^3/_2$ state. The corresponding high spin AF-coupled $\{S_1 = {}^5/_2, S_2 = -2\}$ and $\{S_1 = -2, S_2 = {}^5/_2\}$ states, however, yield longer Fe−Fe distances of 2.804 and 2.762 Å, respectively. These are shorter than the Fe1−Fe2 distances for the current model but are still much longer than the 2.5 Å predicted by the EXAFS measurements. Another crystallized synthetic system is the $[Fe(II)Fe(III)(OH)_3(tmtacn)_2]^{2+}$ cluster, which contains three (OH^-) bridges with ($S_1 = 2$, $S_2 = {}^5/_2$, and $S_{total} = 9/2$) state, and produces a short Fe−Fe distance of 2.51 Å.[53,54] Comparing with these two synthetic systems, it is difficult to see how our current model with an Fe(III)−O−Fe(IV) core, one μ-1,1 carboxylate, and one bidentate carboxylate bridge will produce the 2.5 Å Fe−Fe distance in the (S_a =

(49) Bollinger, J. M., Jr.; Chen, S.; Parkin, S. E.; Mangravite, L. M.; Ley, B. A.; Edmondson, D. E.; Huynh, B. H. *J. Am. Chem. Soc.* **1997**, *119*, 5976−5977.
(50) Dong, Y.; Fujii, H.; Hendrich, M. P.; Leising, R. A.; Pan, G.; Randall, C. R.; Wilkinson, E. C.; Zang, Y.; Que, L., Jr.; Fox, B. G.; Kauffmann, K.; Münck, E. *J. Am. Chem. Soc.* **1995**, *117*, 2778−2792.
(51) Ghosh, A.; Almlöf, J.; Que, L., Jr. *Angew. Chem., Int. Ed. Engl.* **1996**, *35*, 770−772.
(52) Skulan, A. J.; Hanson, M. A.; Hsu, H. Que, L., Jr.; Solomon, E. I. *J. Am. Chem. Soc.* **2003**, *125*, 7344−7356.
(53) Gamelin, D. R.; Bominaar, E. L.; Kirk, M. L.; Wieghardt, K.; Solomon, E. I. *J. Am. Chem. Soc.* **1996**, *118*, 8085−8097.
(54) Gamelin, D. R.; Bominaar, E. L.; Mathoniere, C.; Kirk, M. L.; Wieghardt, K.; Girerd, J.-J.; Solomon, E. I. *Inorg. Chem.* **1996**, *35*, 4323−4335.

2, $S_b = {}^5/_2$, and $S_{total} = {}^1/_2$) state. Further experimental and theoretical studies, therefore, are still needed to provide more structural information about X.

The fact that the DFT-calculated ^{1}H proton and ^{17}O hyperfine couplings for the $\{(OH^-)_t$ ($S_1 = {}^5/_2$, $S_2 = -2)\}$ model are the best among the models studied here in comparing with the experiments supports the earlier proposal based on analysis of ENDOR spectra that the terminal oxygen group is ligated to the Fe(III) site in RNR-X.[16]

Without directly observing the structure for RNR-X, one can only approach the "correct" structure by comparison and contrast, and in that context, this and our earlier work[21] represent the start of a systematic exploration of likely structures and properties. There may be other unusual structures related to RNR-X not yet observed, potentially experimentally accessible by mutagenesis or irradiation. Additional theoretical (computational) work is planned on alternative RNR-X structural models with evaluation of structures, energies, Fe Mössbauer parameters, and quantitative ligand hyperfine calculations.

Acknowledgment. We thank NIH for financial support (GM43278 to L.N.). The generous support of computer time on the SGI clusters of the Scripps Research Institute is gratefully acknowledged.

Appendix: Simple Estimation Methods for Ligand Hyperfine

In Table 2 we give calculated estimates of the ^{1}H (proton) hyperfine coupling on OH^- or H_2O and of the ^{17}O isotropic coupling compared with the experimental values for RNR-X. For the proton hyperfine coupling we have used the local spin dipolar hyperfine coupling model of Willems et al.[16] which they used in their structural analysis. We assumed

$$A = {}^7/_3\,(A_{Fe(III)}) \text{ or } A = -{}^4/_3\,(A_{Fe(IV)}) \qquad (A.1)$$

depending on whether the OH^- or H_2O is coordinated to Fe(III) or Fe(IV). All the spin density is assumed to be localized at Fe(III) or Fe(IV) and acts through space. These are axial dipolar tensors of the form

$$A_3 = {}^7/_3\,(C/r_1{}^3) \text{ or } A_3 = -{}^4/_3\,(C/r_2{}^3) \text{ for } r_1 = \text{Fe(III)}-\text{H or } r_2 = \text{Fe(IV)}-\text{H} \quad (A.2)$$

depending on which of r_1 or r_2 is smaller. The factors ${}^7/_3$ and ${}^4/_3$ are spin projection factors, and A_3 is the largest principal value of the hyperfine tensor directed along r_1 or r_2, respectively. The tensor is axial with other principal values $A_1 = A_2 = -A_3/2$. The constant $C = 2g_e\beta_e g_n\beta_n$.

For our calculations of the ^{17}O isotropic coupling constants, we used the Mulliken valence O(2s) spin populations, Q_s, from the broken symmetry wave functions rescaled by the spin coupling factors $K_A/2S_A$ for Fe(III) ($K_A = {}^7/_3$, $S_A = {}^5/_2$) and $K_B/2S_B$ for Fe(IV) ($K_B = -{}^4/_3$, $S_B = 2$)[35] and with the isotropic coupling constant for one unpaired electron[55] approximated as $A_{iso}(1e^-) = -5309$ MHz for ^{17}O. Therefore

$$A_{iso,calc} = (K_A Q_S(A) A_{iso}(1e^-)/2S_A) \text{ or } (K_b Q_S(A) A_{iso}(1e^-)/2S_B) \quad (A.3)$$

depending on whether the dominant coupling on ^{17}O is due to Fe(III) or Fe(IV). The relative signs of the spin populations on Fe and bridging or terminal oxygens were used to determine these, assuming that minority spin transfer from O to Fe will give the same sign for the spin on oxygen and the dominant Fe site. These results are entirely consistent with shorter Fe−O bridging and Fe−L (OH^- or H_2O) terminal bonds.

IC0206443

(55) Solomon, E. I.; Hanson, M. A. In *Inorganic Electronic Structure and Spectroscopy, Volume II: Applications and Case Studies*; Solomon, E. I., Lever, A. B. P., Eds.; John Wiley and Sons: New York, 1999; Chapter 1, pp 1−130.